RSC Advances

ROYAL SOCIETY OF CHEMISTRY

www.rsc.org/advances

Journal Name

ARTICLE

Improved structural and electrochemical performances of $LiNi_{0.5}Mn_{1.5}O_4$ cathode materials by Cr^{3+} and/or Ti^{4+} doping

Received 00th January 20xx,
Accepted 00th January 20xx

DOI: 10.1039/x0xx00000x

www.rsc.org/

Li Wang, *[abc] Dan Chen, [abc] Jiangfeng Wang, [abc] Guijuan Liu, [abc] Wei Wu [abc] and Guangchuan Liang [abc]

High voltage $LiNi_{0.45}M_{0.05}Mn_{1.5}O_4$ (M = Ni, Cr, Ti, $Cr_{0.5}Ti_{0.5}$) cathode materials were synthesized by solid-state method, and the effects of Cr/Ti doping alone and co-doping on the crystalline structure, Mn^{3+} content, particle morphology and electrochemical performance of $LiNi_{0.5}Mn_{1.5}O_4$ cathode materials were systematically investigated. The as-prepared samples were characterized by XRD, FT-IR, SEM, CV, EIS and galvanostatic charge/discharge cycling tests. XRD results show that both pristine and doped materials have cubic spinel structure with *Fd3m* space group, and the Cr and/or Ti doping can effectively prevent the formation of $Li_yNi_{1-y}O$ impurity phase. FT-IR spectra indicate that the Cr and/or Ti doping increases the disordering degree of Ni/Mn ions in 16d octahedral sites. SEM observation discloses that the Cr and/or Ti doping increases the particle size distribution homogeneity and decreases the average primary particle size. EIS analysis illustrates that the Cr and/or Ti doping decreases the charge transfer resistance and increases the Li^+ ion diffusion coefficient. All of the above-mentioned factors are believed to be advantageous to the cycling stability and rate capability. Among which, the Cr and Ti co-doped sample $LiNi_{0.45}Cr_{0.025}Ti_{0.025}Mn_{1.5}O_4$ exhibits optimal cycling performance with a capacity retention rate of 102.1% after 100 cycles at 1C rate, and optimal rate capability with a discharge capacity of 118.7 mA h g^{-1} at 10 C rate, which is 96.1% of its capacity at 0.2 C rate. The excellent electrochemical performance of $LiNi_{0.45}Cr_{0.025}Ti_{0.025}Mn_{1.5}O_4$ cathode material may be mainly attributed to the presence of appropriate Mn^{3+} content and higher Li^+ ion diffusion coefficient.

Introduction

High voltage $LiNi_{0.5}Mn_{1.5}O_4$ spinel is now a very promising cathode material for lithium ion batteries that can be applied in electric vehicle (EV), hybrid electric vehicle (HEV) and plug-in hybrid electric vehicle (PHEV),[1] due to the advantages of low cost, good rate capability, high energy density and safety characteristics.[2-4] However, the electrochemical properties of $LiNi_{0.5}Mn_{1.5}O_4$ are strongly influenced by Mn^{3+} concentration, Mn dissolution and impurities,[5] which make the synthesis of $LiNi_{0.5}Mn_{1.5}O_4$ with superior performances a challenge.

Up to now, various synthesis methods producing $LiNi_{0.5}Mn_{1.5}O_4$ with different morphologies and electrochemical performances have been reported, such as solid-state,[6,7] sol-gel,[8] co-precipitation,[9,10] molten salt,[11] hydrothermal route,[12,13] etc. Among the above methods, the solid-state method is simple, cheap, and more importantly, easy to realize industrialization. But the high temperature calcination often results in oxygen loss, accompanied with the co-existence of $Li_yNi_{1-y}O$ as an impurity phase, which is disadvantageous to the discharge capacity and cycling stability.[14] In addition, the oxygen loss is usually accompanied with the formation of Mn^{3+} to maintain charge neutrality, whose presence plays double roles. On one hand, Mn^{3+} can increase the electronic and ionic conductivity due to its electrochemical activity.[15,16] On the other hand, part of Mn^{3+} may form Mn^{2+} via the disproportionation reaction, causing significant capacity loss during cycling.[17] Therefore, controlling the appropriate Mn^{3+} content is critical for $LiNi_{0.5}Mn_{1.5}O_4$ cathode material to achieve superior electrochemical performance. To eliminate the $Li_yNi_{1-y}O$ impurity and control the Mn^{3+} content, one of the commonly adopted approaches is to partially substitute Mn and/or Ni with other cations, such as Cu,[18] Zn,[8,18] Fe,[19] Co,[19] Mg,[20] Ru,[21] Cr[22] and Ti.[23,24] The elements Cr and Ti are typical doping ions to modify the $LiNi_{0.5}Mn_{1.5}O_4$ spinel. Zhang et al.[22] have found that Cr^{3+}-doping could effectively eliminate the $Li_yNi_{1-y}O$ impurity phase and improve structural stability. Wang et al.[24] have synthesized $LiNi_{0.4}Ti_{0.1}Mn_{1.5}O_4$ by solid-state reaction and found that $LiNi_{0.5}Mn_{1.5}O_4$ has higher crystallinity, discharge capacity and cycling retention rate after Ti doping. Although the

[a] Institute of Power Source and Ecomaterials Science, Hebei University of Technology, Tianjin 300130, China. E-mail: wangli_hebut@163.com
[b] Key Laboratory of Special Functional Materials for Ecological Environment and Information (Hebei University of Technology), Ministry of Education, Tianjin 300130, China.
[c] Key Laboratory for New Type of Functional Materials in Hebei Province, Hebei University of Technology, Tianjin 300130, China.

substitution of them can improve the performance of $LiNi_{0.5}Mn_{1.5}O_4$, it is hard to identify which is the most effective from these literatures due to the different synthesis methods and test standards from group to group. Therefore, in this study, we have systematically investigated the effects of doping Cr and Ti alone or both for Ni element on the crystalline structure, Mn^{3+} content, particle morphology and electrochemical performance of $LiNi_{0.5}Mn_{1.5}O_4$ cathode materials prepared by the same solid-state method, to gain a further insight into the impacts of cation doping.

Experimental

Material synthesis.

Pristine $LiNi_{0.5}Mn_{1.5}O_4$ was synthesized by ball milling the mixture of stoichiometric Li_2CO_3 (1.5221 g), NiO (1.4938 g) and Mn_3O_4 (4.5764 g) for 1 h followed by calcination at 500 °C for 5 h and 850 °C for 8 h under air atmosphere with a heating rate of 5 °C min^{-1}, and the thus obtained cathode material was labelled as LNMO. Cr_2O_3 and TiO_2 were used as the sources of doping ions and added in the starting materials to give the final compositions of $LiNi_{0.45}Cr_{0.05}Mn_{1.5}O_4$ (Cr_2O_3: 0.1535 g, NiO: 1.3444 g), $LiNi_{0.45}Ti_{0.05}Mn_{1.5}O_4$ (TiO_2: 0.1614 g, NiO: 1.3444 g) and $LiNi_{0.45}Cr_{0.025}Ti_{0.025}Mn_{1.5}O_4$ (Cr_2O_3: 0.0767 g, TiO_2: 0.0807 g, NiO: 1.3444 g), which were named as LNMO-Cr, LNMO-Ti and LNMO-CrTi, respectively. To compensate for the lithium loss during high temperature calcination, 3 mol.% extra amount of lithium source was used in all the starting materials.

Characterization and electrochemical measurements.

A powder X-ray diffractometer (D8-FOCUS, Bruker, Germany) equipped with a Cu Kα radiation source (λ = 0.15406 nm) was used to study the structural properties. The morphology and particle size distribution of the materials were analyzed by scanning electron microscopy (Nova Nano SEM450, FEI, USA). Fourier Transformation Infrared Spectrometer (V80, Bruker, Germany) was used to identify the Ni/Mn ordering distribution in $LiNi_{0.5}Mn_{1.5}O_4$ material with a wavenumber scale of 400-700 cm^{-1}.

To fabricate the positive electrode, the as-prepared cathode materials were mixed with ethylene black and polytetrafluoroethylene (PTFE) in a mass ratio of 80:15:5. The CR2032 test coin cells were assembled in an argon-filled glove box using lithium foil as the counter electrode, polypropylene microporous membrane as the separator and 1 M $LiPF_6$ dissolved in ethylene carbonate (EC) - dimethyl carbonate (DMC) - ethyl methyl carbonate (EMC) (1:1:1, v/v/v) as the electrolyte. The cells were charged and discharged galvanostatically at different current densities (1C = 147 mA h g^{-1}) using the Land battery test system CT2001A (Land, Wuhan, China) in a voltage range of 3.5-4.95 V (*vs.* Li/Li^+). Cyclic voltammetry and electrochemical impedance spectroscopy (EIS) were conducted using an electrochemical workstation (CHI660, Shanghai, China). The CV curves were recorded in the voltage range of 3.3-5.0 V (*vs.* Li/Li^+) at a scanning rate of 0.1 mV s^{-1}. The electrochemical impedance spectra were recorded by applying an ac amplitude of 5 mV over a frequency range from 10 mHz to 100 kHz at fully-discharged state after rate capability test.

Results and discussion

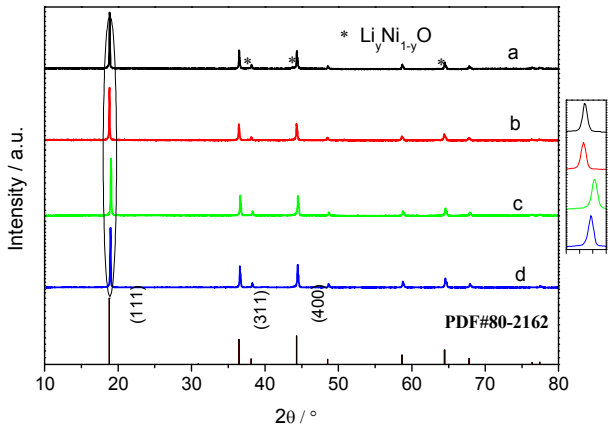

Fig. 1 XRD patterns of (a) $LiNi_{0.5}Mn_{1.5}O_4$; (b) $LiNi_{0.45}Cr_{0.05}Mn_{1.5}O_4$; (c) $LiNi_{0.45}Ti_{0.05}Mn_{1.5}O_4$; (d) $LiNi_{0.45}Cr_{0.025}Ti_{0.025}Mn_{1.5}O_4$. The right graph is the magnified image of (111) peak.

Fig. 1 shows the XRD patterns of the pristine and doped $LiNi_{0.5}Mn_{1.5}O_4$ samples. All the diffraction peaks can be ascribed to cubic spinel structure (JCPDS card No. 80-2162) with a space group of *Fd3m*, in which lithium ions occupy the tetrahedral (8*a*) sites, transition metals (Ni, Cr, Ti and Mn) are located at the octahedral (16*d*) sites, and oxygen atoms reside in the 32*e* sites. The sharp and narrow peaks imply high crystallinity of the materials. But for the pristine LNMO sample, in addition to the major spinel phase, there also exist weak reflections at ~37.6, 43.8 and 63.4°, corresponding to the impurity phase $Li_yNi_{1-y}O$ with rock salt structure, due to the oxygen loss during high temperature calcination.[25] However, the three doped samples exhibit higher phase purity with lower impurity content, as shown in Fig. S1 (ESI†), which is consistent with earlier reports that the cation doping could effectively suppress the formation of $Li_yNi_{1-y}O$ impurity phase and stabilize the spinel crystal structure.[26,27] The high phase purity is believed to be advantageous to the enhancement of discharge capacity and cycling stability. In addition, from the magnified pattern of (111) peak, it can be clearly seen that compared to pristine LNMO sample, the diffraction peak

of Cr-doped sample LNMO-Cr shifts slightly to lower degree direction, while those of Ti-doped and Cr/Ti co-doped samples shift to higher degree direction. This phenomenon can be explained by the different ionic radii of Ni^{2+} (0.69 Å, four-coordination), Cr^{3+} (0.76 Å, six-coordination), Ti^{4+} (0.56 Å, four-coordination) based on Bragg equation $2d\sin\theta=n\lambda$. To further investigate the structural change, lattice parameters calculated from XRD are summarized in Table 1. It can be seen that the lattice parameters of LNMO, LNMO-Cr, LNMO-Ti and LNMO-CrTi are 8.1652, 8.1712, 8.1328 and 8.1590 Å, respectively. The increase of lattice parameter after Cr-doping may be due to that the substitution of Cr^{3+} for Ni^{2+} leads to the partial reduction of smaller Mn^{4+} (0.67 Å) to larger Mn^{3+} (0.72 Å) for the sake of charge compensation. Additionally, the larger ionic radii of Cr^{3+} compared to Ni^{2+} also lead to its larger lattice parameter. However, both Ti-doped and Cr/Ti co-doped samples show decreased lattice parameters, which may be due to the smaller values of r_{Ti4+} and $(r_{Cr3+} + r_{Ti4+}) / 2$ (0.66 Å) compared to r_{Ni2+}. In the meantime, the difference in lattice parameters also demonstrates the incorporation of Cr and/or Ti into the spinel crystal lattice.

Table 1 Lattice parameters (a, V), crystallite sizes (D) and I_{400}/I_{311} values of $LiNi_{0.45}M_{0.05}Mn_{1.5}O_4$ (M = Ni, Cr, Ti, $Cr_{0.5}Ti_{0.5}$) samples

Sample	a (Å)	V (Å)	D (nm)	I_{400}/I_{311}
LNMO	8.1652	544.38	69.48	1.038
LNMO-Cr	8.1712	545.58	65.79	1.141
LNMO-Ti	8.1328	537.92	64.28	1.183
LNMO-CrTi	8.1590	543.13	64.83	1.147

Based on Scherrer equation $D=k\lambda/\beta\cos\theta$, where k is 0.89, λ is 0.15406 nm and β is the full-width-at-half-maximum (FWHM) of the diffraction peak on a 2θ scale, we can get the crystallite size (D) of the pristine and doped $LiNi_{0.5}Mn_{1.5}O_4$ cathode materials according to D_{111}, D_{400} and D_{311} values, which are also listed in Table 1. From the table we can see that the crystallite sizes of LNMO, LNMO-Cr, LNMO-Ti and LNMO-CrTi are 69.48, 65.79, 64.28 and 64.83 nm, respectively, illustrating that the doped samples have a smaller crystallite size, which may be due to the inhibition of crystallite growth by the doping ions. The smaller crystallite size is believed to be advantageous to the rate capability due to the shortened Li^+ ion diffusion length, which can be verified by the following SEM observation.

Many researchers[28-30] have reported that the integrated intensity ratio of (400)/(311) peak reflects the extent of occupancy of the heavier ions in the 8*a* lithium sites, which would lead to unfavorable electrochemical characteristics. From Fig. 1 we can get the integrated intensity ratios of (400)/(311) for LNMO, LNMO-Cr, LNMO-Ti and LNMO-CrTi are 1.038, 1.141, 1.183 and 1.147, respectively, as listed in Table 1, and the lower intensity ratio of (400)/(311) for the pristine LNMO sample suggests that the transition metal ions show a propensity to occupy the 8*a* lithium sites in $LiNi_{0.5}Mn_{1.5}O_4$ due to the $Li_yNi_{1-y}O$ impurity, that is, the pristine LNMO sample has a higher cation mixing degree, and the presence of transition metal ions with larger ionic radii in the Li site will hamper the Li^+ ion diffusion, which is believed to be detrimental to electrochemical performance.

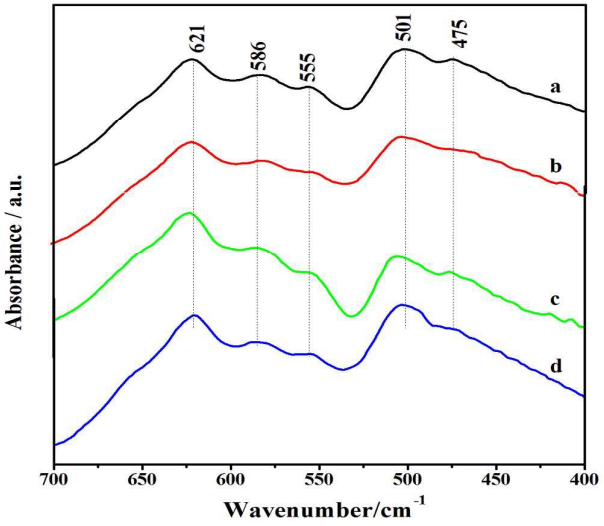

Fig. 2 FT-IR spectra of (a) $LiNi_{0.5}Mn_{1.5}O_4$; (b) $LiNi_{0.45}Cr_{0.05}$-$Mn_{1.5}O_4$; (c) $LiNi_{0.45}Ti_{0.05}Mn_{1.5}O_4$; (d) $LiNi_{0.45}Cr_{0.025}Ti_{0.025}Mn_{1.5}O_4$

$LiNi_{0.5}Mn_{1.5}O_4$ spinel has two different space groups, disordered *Fd3m* and ordered $P4_332$, which are characterized by the random distribution of Ni and Mn in octahedral 16*d* sites and the ordered occupation of Ni and Mn in octahedral 4*a* and 12*d* sties, respectively. It is difficult to observe the structural difference between these two space groups by XRD, due to the similar scattering factors of Ni and Mn. Instead, FT-IR has been proven to be an effective technique for analyzing the cation ordering.[15,31-33] $LiNi_{0.5}Mn_{1.5}O_4$ with $P4_332$ space group typically produces a fingerprint FT-IR spectrum consisting of eight well-defined bands at 432, 468, 478, 503, 557, 594, 621 and 648 cm^{-1},[34] whereas disordered *Fd3m* phase gives a rather broad spectrum with only five bands.[31] As shown in Fig. 2, the spectra of the pristine and doped samples between 700 and 400 cm^{-1} are very similar. The two bands at 621 and 501 cm^{-1} are more intensive than those at 586 and 475 cm^{-1}, respectively. In addition, the two bands at 648 and 432 cm^{-1}, characteristic for $P4_332$ phase, are absent or undefined. These features indicate that all the four samples have disordered structure with *Fd3m* space group,[32] in good consistence with the XRD results.

Additionally, it has been reported that the ordering in 16*d* octahedral sites can be qualitatively determined by the intensity ratio between the peaks at 586 and 621 cm^{-1}.[31] Specifically, the

intensity of the 586 cm^{-1} Ni-O band increases compared to that of the 621 cm^{-1} Mn-O band as the degree of ordering in the 16*d* sites increases. As we can see in Fig. 2, the relative intensity of the 586 cm^{-1} Ni-O band decreases after doping, indicating a decrease in the cation ordering degree in the 16*d* octahedral sites. According to Ref. 19, the difference in the cation disordering degree can be attributed to the size difference between doping cation and Mn^{4+}. Therefore, the different cation disordering degree of the doped samples may be attributed to the cation radius difference between Cr^{3+}, Ti^{4+} and Mn^{4+}. To some extent, the decrease of cation ordering degree may be due to the presence of Mn^{3+}, and the lower the cation ordering degree, the higher Mn^{3+} content. Based on the FT-IR spectra, we can get the intensity ratios between 586cm^{-1}/621cm^{-1} for LNMO, LNMO-Cr, LNMO-Ti and LNMO-CrTi are 0.883, 0.880, 0.693 and 0.859, respectively, that is, the cation disordering degree and relative Mn^{3+} content decrease in the following order: LNMO-Ti > LNMO-CrTi > LNMO-Cr > LNMO. The relative Mn^{3+} content in the product is relevant to the valence of doping ions under the conditions of the same doping amount. The higher the valence of doping ions, the more Mn^{3+} ions will be formed in order to maintain charge neutrality. The increase of Mn^{3+} content of the Cr-doped sample in this study is consistent with Ref. 19,35, but contrary to Ref. 28, which may be due to the different synthesis method and doping amount.

In addition to the superstructure reflections in XRD and the FT-IR bands normally used to assess the cation ordering, it has been reported in Ref. 19 that an examination of the charge/discharge behavior below 3 V involving the insertion/extraction of Li^+ ions into/from the empty 16*c* sites is an effective way to assess precisely the cation ordering degree in the 5 V spinels. The first discharge and second charge profiles, along with the differential capacity plots of the pristine and doped $LiNi_{0.5}Mn_{1.5}O_4$ samples at 0.2 C rate are shown in Fig. 3. Due to the higher polarization at low voltages below 2.5 V, those samples were discharged below 2 V until the discharge capacity reached twice the value of the discharge capacity at 3.5 V to equally utilize both the 8*a* tetrahedral sites and 16*c* octahedral sites of the spinel lattice.[19,36] From the first discharge curves in Fig. 3(a), it can be seen that all samples show distinct plateaus at ~4.7 V and ~4.0 V, corresponding to the Li^+ ion insertion into the 8*a* tetrahedral sites,[36,37] which can be clearly seen in *d*Q/*d*V curves in Fig. 3(c). From Fig. 3(a) we can also see that all doped samples exhibit a longer ~4.0 V plateau compared to that of the pristine sample due to an increase in Mn^{3+} content resulting from the substitution of Cr^{3+} and/or Ti^{4+} for Ni^{2+}.[38] Besides that, the two plateaus at ~2.7 V and ~2.1 V can be attributed to the reduction of Mn^{4+} to Mn^{3+} involving Li^+ ion insertion into empty 16*c* octahedral sites, which is associated with the evolution of two tetragonal phases from the cubic phase.[36] Manthiram et al.

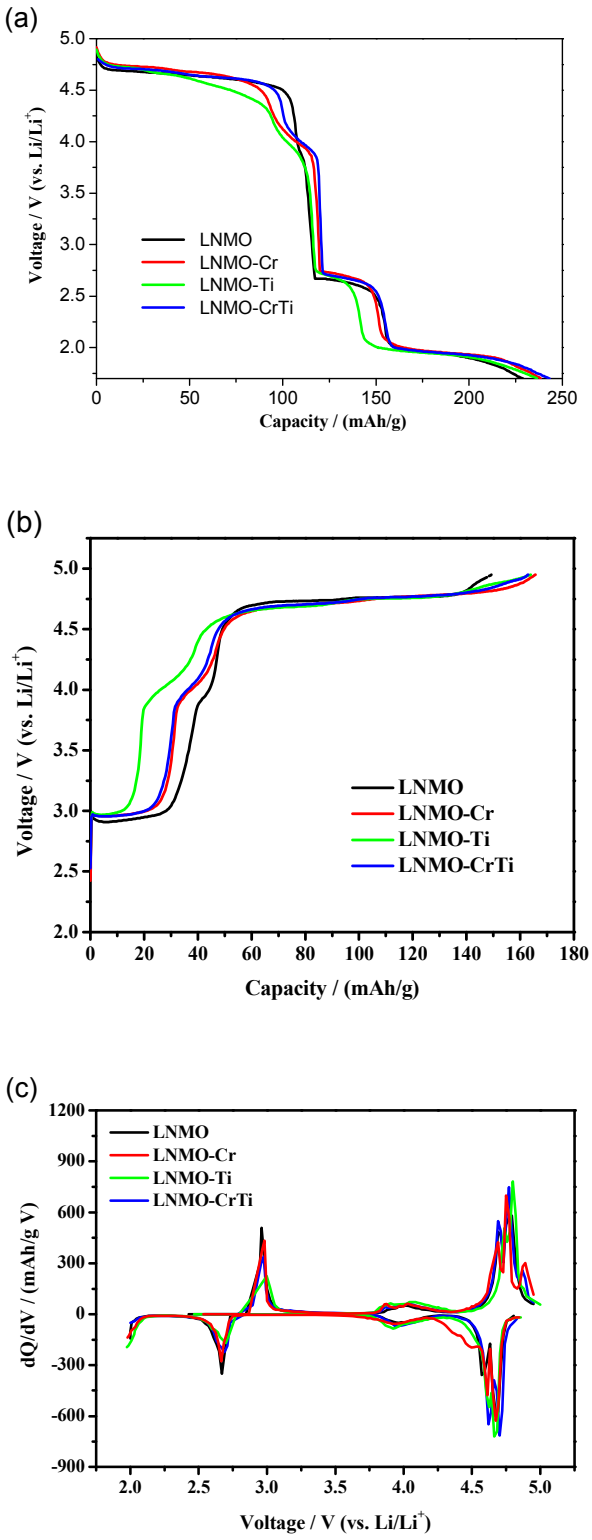

Fig. 3 (a) First discharge profiles, (b) second charge profiles, and (c) differential capacity (dQ/dV) plots of $LiNi_{0.45}M_{0.05}Mn_{1.5}O_4$ (M = Ni, Cr, Ti, $Cr_{0.5}Ti_{0.5}$) samples between 5 and 2 V at 0.2 C rate

demonstrated that the relative capacity variation at the ~2.7 V and ~2.1 V can be used to determine qualitatively the relative cation ordering degree in the spinels,[19,36] and the capacity at the ~2.7 V plateau increases at the expense of the capacity at the ~2.1 V plateau as the cation ordering degree increases. The first discharge capacity variations of all the samples between the ~2.7 V to ~2.1 V plateaus are compared in Table 2. From Fig. 3(a) and Table 2 we can see that the pristine LNMO sample shows the longest plateau at ~2.7 V, indicating its higher cation ordering degree. As for the doped samples, the relative ordering degree varies in the following order: LNMO-Cr > LNMO-CrTi > LNMO-Ti, which is in consistence with the above FT-IR results.

Table 2 Comparison of the first discharge capacities of $LiNi_{0.45}M_{0.05}Mn_{1.5}O_4$ (M = Ni, Cr, Ti, $Cr_{0.5}Ti_{0.5}$) samples

	First discharge capacity (mA h g^{-1})				
			Capacity below 3 V		
Sample	Total	Capacity above 3.5 V	Total	~2.7 V plateau	~2.1 V plateau
LNMO	229.0	115.9	113.1	41.8	71.3
LNMO-Cr	238.3	119.5	118.8	33.8	85.0
LNMO-Ti	236.5	116.5	120.0	26.6	93.4
LNMO-CrTi	242.9	120.9	122.0	33.6	88.4

As for the second charge curves, as shown in Fig. 3(b), two plateaus (~2.9 and ~3.8 V) appear when Li^+ ions are removed from the 16*c* octahedral sites,[36] and the capacity at the ~3.8 V plateau increases as the cation ordering degree decreases. Therefore, it can be concluded that the cation ordering degree varies in the order of LNMO > LNMO-Cr > LNMO-CrTi > LNMO-Ti, well consistent with the FT-IR results. The increase of cation disordering degree after Cr and/or Ti doping is mainly caused by the presence of more Mn^{3+} ions in the product. Additionally, from the *d*Q/*d*V curves in Fig. 3(c) it can be clearly seen that LNMO-Cr and LNMO-CrTi samples show a small peak at ~4.9 V during Li^+ ion insertion due to the reduction of Cr^{4+} to Cr^{3+},[30] and the sample doped with Cr^{3+} alone exhibits a higher peak intensity at ~4.9 V due to more Cr^{3+} in the product.

Fig. 4 shows the SEM images of the pristine and doped $LiNi_{0.5}Mn_{1.5}O_4$ cathode materials. It can be seen that the pristine and doped samples exhibit similar particle morphology, which are secondary aggregates composed of octahedral primary particles. The surface facets of the octahedrons correspond to (111) crystal planes, which is thermodynamically more stable.[39] From Fig. 4(b) we can see that the pristine LNMO sample shows various crystallite sizes with incomplete crystal growth. However, the Cr and/or Ti doping obviously improves the uniformity of crystal morphology, including fine, uniform crystallite size and reduced agglomeration, which is well consistent with the crystallite size obtained from XRD.

The particle size distribution curves of pristine LNMO and co-doped LNMO-CrTi samples are shown in Fig. S2 (ESI†), whose D_{10}, D_{50}, D_{90} values are listed in Table S1 (ESI†). It is generally accepted that the smaller the $(D_{90}- D_{10})/D_{50}$ value is, the narrower the particle size distribution is. From the table it can be seen that the co-doped sample (LNMO-CrTi) exhibits smaller D_{50} and $(D_{90}- D_{10})/D_{50}$ values than the pristine sample (LNMO), confirming its smaller average particle size with narrower particle size distribution, which is believed to be advantageous to the electrochemical performance due to the reduced Li^+ ion diffusion distance and enlarged active specific surface area.

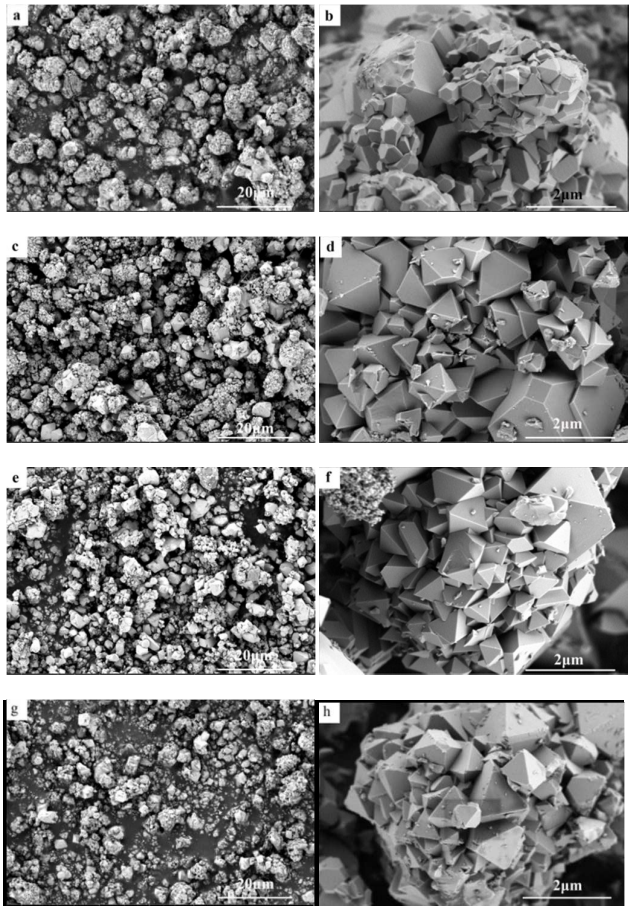

Fig. 4 SEM images of (a,b) $LiNi_{0.5}Mn_{1.5}O_4$; (c,d) $LiNi_{0.45}Cr_{0.05}Mn_{1.5}O_4$; (e,f) $LiNi_{0.45}Ti_{0.05}Mn_{1.5}O_4$; (g,h) $LiNi_{0.45}Cr_{0.025}Ti_{0.025}Mn_{1.5}O_4$

High rate performance is one of the most important electrochemical properties of lithium ion batteries for high power applications.[40-42] Therefore, the rate capabilities of the pristine and doped $LiNi_{0.5}Mn_{1.5}O_4$ samples are evaluated at different rates of 0.2 C, 1 C, 5 C and 10 C, as shown in Fig. 5. From the figure we can see that with increasing current density, the discharge capacities of all samples gradually decrease because of the high polarization caused by kinetic limitations. From Fig. 5(a) it can be seen that the rate

capability is improved to different extent by the Cr^{3+} and/or Ti^{4+} doping. The ratio of discharge capacity at 10 C rate to that at 0.2 C rate increases from 86.2% for LNMO to 88.7% for LNMO-Cr, 91.1% for LNMO-Ti and 96.1% for LNMO-CrTi, respectively. Furthermore, from the discharge curves in Fig. 5(b) we can also see that the discharge voltage platforms of the doped samples are enhanced compared with that of the pristine one, especially at high current densities of 5 C and 10 C, indicating that the polarization is effectively suppressed and the rate capability is obviously improved by the Cr^{3+} and/or Ti^{4+} doping, which can also be verified from the charge curves at 5 C rate, as shown in Fig. S3 (ESI†), for that the charge voltage plateau decreases to different extent after Cr and/or Ti doping. It has been reported that the polarization at high current density is usually caused by limited electronic conductivity and slow Li^+ ions transfer rate.[43] Therefore, the decreased polarization of the doped samples may be due to the reduced particle size and enhanced electronic conductivity resulting from the presence of more Mn^{3+} in the products.

The lower discharge capacity at 0.2 C rate may be due to the incomplete dispersion of electrolyte into the electrode at the beginning, or more side reactions between electrode and electrolyte resulting from longer charge/discharge time. Additionally, from the discharge curves at 0.2 C rate, we can see that all samples exhibit large discharge plateaus at 4.7 V, which can be ascribed to the Ni^{2+}/Ni^{4+} redox couple. And the presence of small plateaus at 4.0 V is caused by the Mn^{3+}/Mn^{4+} redox couple. The capacity of this plateau can be qualitatively used to evaluate the relative Mn^{3+} content in the spinels, which can be calculated from the discharge capacity between 3.8 and 4.25 V divided by the total discharge capacity.[5] Therefore, based on the discharge curves at 0.2 C rate, we can get that the relative Mn^{3+} contents of LNMO, LNMO-Cr, LNMO-Ti and LNMO-CrTi are 11.27, 13.65, 18.92 and 15.87%, respectively. It has been reported that the presence of appropriate Mn^{3+} content is critical to accelerate the Li^+ ion transport within the crystalline structure, which is beneficial to enhance the electrochemical properties of $LiNi_{0.5}Mn_{1.5}O_4$ cathode material. $LiNi_{0.5}Mn_{1.5}O_4$ with an appropriate amount of disordered phase offers high rate capability and excellent cycling performance.[14] Therefore, the optimal rate capability of $LiNi_{0.45}Cr_{0.025}Ti_{0.025}Mn_{1.5}O_4$ sample may be partly attributed to the presence of appropriate Mn^{3+} content.

Fig. 6 shows the cyclic voltammograms of the cells with the $LiNi_{0.5}Mn_{1.5}O_4$ and $LiNi_{0.45}M_{0.05}Mn_{1.5}O_4$ (M = Cr, Ti, $Cr_{0.5}Ti_{0.5}$) spinels as the working electrodes. On both cathodic and anodic runs, two peaks are observed at around 4.6-4.8 V, corresponding to the redox reactions of Ni^{2+}/Ni^{3+} and Ni^{3+}/Ni^{4+} couples. Generally, $LiNi_{0.5}Mn_{1.5}O_4$ with *P4₃32* space group shows only a strong oxidation peak around 4.7 V, but the oxidation peak splits into two separate peaks in the *Fd3m* spinel because the voltage difference between Ni^{2+}/Ni^{3+} and Ni^{3+}/Ni^{4+} redox couples is enhanced in the nonstoichiometric spinel.[44-46] This reveals that both pristine and doped samples are with dominant *Fd3m* space group, in consistence with the XRD and FT-IR data. In addition, the separation between the Ni redox couples is determined to be 57, 70, 60 and 62 mV for LNMO, LNMO-Cr, LNMO-Ti and LNMO-CrTi, respectively. As the reported values for peak separation in $LiNi_{0.5}Mn_{1.5}O_4$ samples with disordered and ordered structures are 60 and 20 mV, respectively,[39,47] the results further confirm the disordered structure of the as-prepared samples. The peak at ~4.0 V is related to the Mn^{4+}/Mn^{3+} redox couple, whose peak intensity can roughly represent the relative Mn^{3+} content in the spinel structure. From the magnified graph in the inset of Fig. 6 it can be concluded that

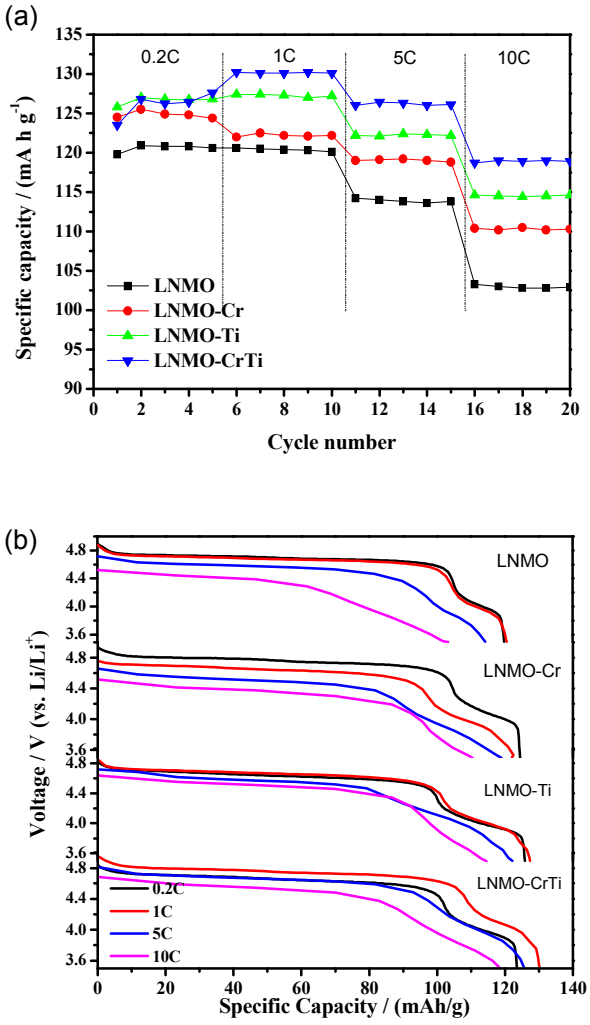

Fig. 5 Rate performance (a) and discharge curves at different rates (b) of $LiNi_{0.45}M_{0.05}Mn_{1.5}O_4$ (M = Ni, Cr, Ti, $Cr_{0.5}Ti_{0.5}$) samples

the relative Mn^{3+} contents increase in the order of LNMO < LNMO-Cr < LNMO-CrTi < LNMO-Ti, in good accordance with FT-IR result and first discharge behavior below 3 V. In addition, the CV profile of LNMO-CrTi exhibits higher peak current density and more symmetrical redox peaks than other three samples, indicating the enhanced electrode reactivity,[48] which leads to its better electrochemical performance.

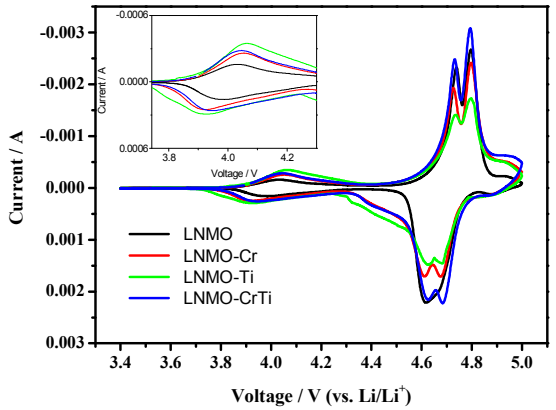

Fig. 6 Cyclic voltammograms of $LiNi_{0.45}M_{0.05}Mn_{1.5}O_4$ (M = Ni, Cr, Ti, $Cr_{0.5}Ti_{0.5}$) samples. The inset is the magnified image of ~4.0 V peak.

It is generally accepted that the polarization degree can be measured by the potential difference (Δϕ) between the anodic (ϕ_a) and cathodic (ϕ_c) peaks of $LiNi_{0.5}Mn_{1.5}O_4$, which is listed in Table 3. From Table 3 we can see that the voltage differences between the oxidation and reduction peaks for both Ni^{2+}/Ni^{3+} and Ni^{3+}/Ni^{4+} redox couples decrease in the order of LNMO > LNMO-Cr > LNMO-Ti > LNMO-CrTi, that is, the doped samples have smaller oxidation/reduction voltage differences, implying faster Li^+ ion transfer and higher reversibility of the electrochemical reactions,[16] thus leading to their higher discharge capacity and rate capability, as shown in Fig. 5.

Table 3 Values of anodic peak (ϕ_a), cathodic peak (ϕ_c) and potential difference (Δϕ) for $LiNi_{0.45}M_{0.05}Mn_{1.5}O_4$ (M = Ni, Cr, Ti, $Cr_{0.5}Ti_{0.5}$) samples

Sample		ϕ_a / V	ϕ_c / V	Δϕ / mV
LNMO	Ni^{2+}/Ni^{3+}	4.739	4.618	121
	Ni^{3+}/Ni^{4+}	4.796	4.665	131
LNMO-Cr	Ni^{2+}/Ni^{3+}	4.727	4.612	115
	Ni^{3+}/Ni^{4+}	4.797	4.676	121
LNMO-Ti	Ni^{2+}/Ni^{3+}	4.734	4.629	109
	Ni^{3+}/Ni^{4+}	4.794	4.681	113
LNMO-CrTi	Ni^{2+}/Ni^{3+}	4.731	4.627	104
	Ni^{3+}/Ni^{4+}	4.793	4.684	109

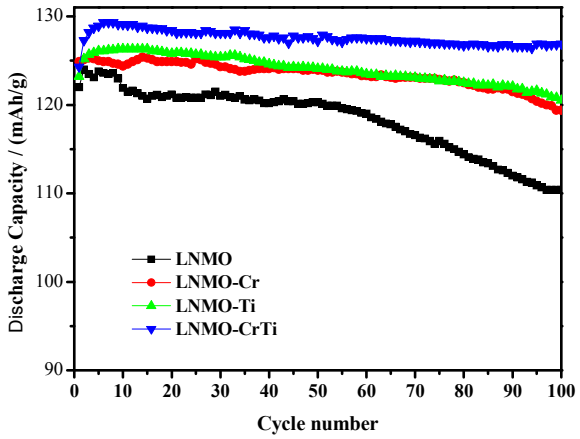

Fig. 7 Cyclic performance curves of $LiNi_{0.45}M_{0.05}Mn_{1.5}O_4$ (M = Ni, Cr, Ti, $Cr_{0.5}Ti_{0.5}$) samples at 1C rate

Table 4 Discharge performance data of $LiNi_{0.45}M_{0.05}Mn_{1.5}O_4$ (M = Ni, Cr, Ti, $Cr_{0.5}Ti_{0.5}$) samples

Sample	Discharge capacity (mA h g^{-1})		Capacity retention rate (%)
	1^{st} cycle	100^{th} cycle	
LNMO	122.0	110.4	90.5
LNMO-Cr	124.9	119.4	95.6
LNMO-Ti	123.2	120.5	97.8
LNMO-CrTi	124.3	126.9	102.1

Fig. 7 shows the cycling performance curves of the pristine and doped $LiNi_{0.5}Mn_{1.5}O_4$ samples at 1 C rate for 100 cycles, whose discharge capacities at 1^{st} and 100^{th} cycle and corresponding retention rates are listed in Table 4. From Table 4 we can see that the capacity retention rates of LNMO, LNMO-Cr, LNMO-Ti and LNMO-CrTi are 90.5, 95.6, 97.8 and 102.1% after 100 cycles, respectively, indicating the better electrochemical reversibility and structural stability of the doped samples. The excellent cycling performance of the doped samples may be explained by the following two reasons. On one hand, it has been reported that Cr element may readily segregate to the particle surface,[19,49] leading to the enrichment of Cr on the surface, which could minimize the contact of Mn^{3+} with the electrolyte and thereby suppress the disproportionation reaction of Mn^{3+} ($Mn^{3+} = Mn^{4+} + Mn^{2+}$) and Mn^{2+} dissolution, although the substitution of Cr^{3+} for Ni^{2+} increases Mn^{3+} content in the spinel structure. And Kim et al.[50] showed that Ti substitution for Mn could reduce electrolyte oxidation and retard some of the degradative parasitic reactions at electrode/electrolyte interface during battery operation. On the other hand, because the Gibbs energy of the formation of NiO, Cr_2O_3 and TiO_2 is -211.7, -1058.1 and -888.8 kJ mol^{-1}, respectively, the bonding strength

between the transition metal elements and oxygen can be strengthened by the incorporation of Cr^{3+} and/or Ti^{4+}, thus reinforcing the spinel framework during cycling.[51,52]

It is generally accepted that the electrochemical performance of high voltage $LiNi_{0.5}Mn_{1.5}O_4$-based spinels depends on many factors, such as phase purity, crystallinity, morphology, particle size and distribution, cation ordering degree, Mn^{3+} content and surface planes in contact with the electrolyte.[53,54] Due to the similar particle morphology with (111) crystallographic planes in contact with the electrolyte, the better rate capability and cycling stability of the doped samples may be attributed to the following reasons: (1) Higher phase purity with lower impurity content. On one hand, the existence of impurity phase without electrochemical activity in the pristine LNMO sample may decrease the amount of active materials. On the other hand, the impurity phase is reported to be more readily to react with the electrolyte.[55] (2) More homogeneous particle size distribution with smaller particle size. This could provide larger specific surface area and shorter Li^+ ion diffusion distance. (3) More disordered *Fd3m* crystal structure induced by the increased Mn^{3+} content. It has been reported that the disordered spinels have higher electronic conductivity and Li^+ ion diffusion coefficient.[11,56] Additionally, the disordered *Fd3m* phase only undergoes a one-step phase transition between two cubic phases during electrochemical cycling, whereas the ordered spinel undergoes two-step phase transitions between three cubic phases.[11] A larger number of phase transformation steps can lead to a higher strain energy during cycling, thus resulting in the worse structural stability of ordered phase. Among the three doped samples, the Cr and Ti co-doped sample $LiNi_{0.45}Cr_{0.025}Ti_{0.025}Mn_{1.5}O_4$ exhibits the optimal electrochemical performance, which may be partly due to the appropriate cation disordering degree, that is, the presence of appropriate Mn^{3+} content. It is generally accepted that the presence of Mn^{3+} ions has dual functions.[57,58] On one hand, the presence of Mn^{3+} could increase both the electronic conductivity and Li^+ ion transportation,[58,59] which is conductive to the rate capability. On the other hand, too many Mn^{3+} ions would lead to disproportionation reactions that produce soluble Mn^{2+} in the electrolyte, which may cause severe capacity fading, especially when full cells are used.[60] Therefore, the presence of appropriate Mn^{3+} content is necessary to the excellent electrochemical performance, which is also reported in Ref. 14,16,61. From the above FT-IR and first discharge behavior below 3 V we know that the co-doped sample LNMO-CrTi has an appropriate cation disordering degree or Mn^{3+} content between the Cr-doped sample LNMO-Cr and Ti-doped sample LNMO-Ti, thus leading to its better overall electrochemical performance.

The electrochemical Li^+ ion insertion/extraction kinetics of $LiNi_{0.5}Mn_{1.5}O_4$ cathode materials were also investigated by means of EIS. Nyquist plots and fitting curves of the as-prepared samples are shown in Fig. 8(a). The equivalent circuit used to fit impedance spectra is shown in the inset. From Fig. 8(a) we can see that all the Nyquist plots are composed of a depressed semicircle in the medium-frequency region followed by a straight line in the low-frequency region. The intercept impedance on the real axis corresponds to the solution resistance (R_e), which is almost the same because of the same electrolyte used in this study. The semicircle in the medium-frequency region represents the charge transfer resistance (R_{ct}). The straight line in the low-frequency region is attributed to the Li^+ ion diffusion into the bulk electrode material or so-called Warburg diffusion. As shown in Fig. 8(a), the fitting line is well coincident with the original data, proving the high credibility of the fitting curve. Table 5 lists the R_{ct} values obtained based on the equivalent circuit, which are 36.81, 23.83, 34.87 and 15.21 Ω for LNMO, LNMO-Cr, LNMO-Ti and LNMO-CrTi, respectively. It can be seen that the Cr and/or Ti doping leads to the obvious decrease of charge transfer resistance, which may be caused by two factors. One is that the presence of more Mn^{3+} ions in the doped sample increases the electronic and ionic conductivity. The other is that the three doped samples have a more uniform particle size distribution with smaller particle size, which increases the contact surface area between the electrode and electrolyte. The decrease of charge transfer resistance is believed to be conductive to the electrochemical performance, especially rate capability and cycling stability.[62]

Table 5 Charge transfer resistance (R_{ct}), σ values and Li^+ ion diffusion coefficients (D_{Li}) for $LiNi_{0.45}M_{0.05}Mn_{1.5}O_4$ (M = Ni, Cr, Ti, $Cr_{0.5}Ti_{0.5}$) samples obtained by EIS

Sample	R_{ct} (Ω)	σ ($\Omega\ s^{-1/2}$)	D_{Li} ($cm^2\ s^{-1}$)
LNMO	36.81	62.798	8.807×10^{-11}
LNMO-Cr	23.83	59.143	1.353×10^{-10}
LNMO-Ti	34.87	39.155	2.012×10^{-10}
LNMO-CrTi	15.21	14.945	5.736×10^{-10}

Previous studies have demonstrated that the apparent chemical diffusion coefficient of Li^+ ions is inversely proportional to the Warburg factor, which can be obtained from the straight line in the low-frequency region using the following equation:[63,64]

$$D_{Li} = R^2T^2/2A^2n^4F^4C^2\sigma^2 \quad (1)$$

where R is the gas constant, T is the absolute temperature, A is the surface area of the electrode, n is the number of electrons per molecule during oxidation, F is the Faraday constant, C is the concentration of Li^+ ions, and σ is the Warburg factor, which has a relationship with Z':

$$Z' = R_{ct} + R_e + \sigma\omega^{-1/2} \quad (2)$$

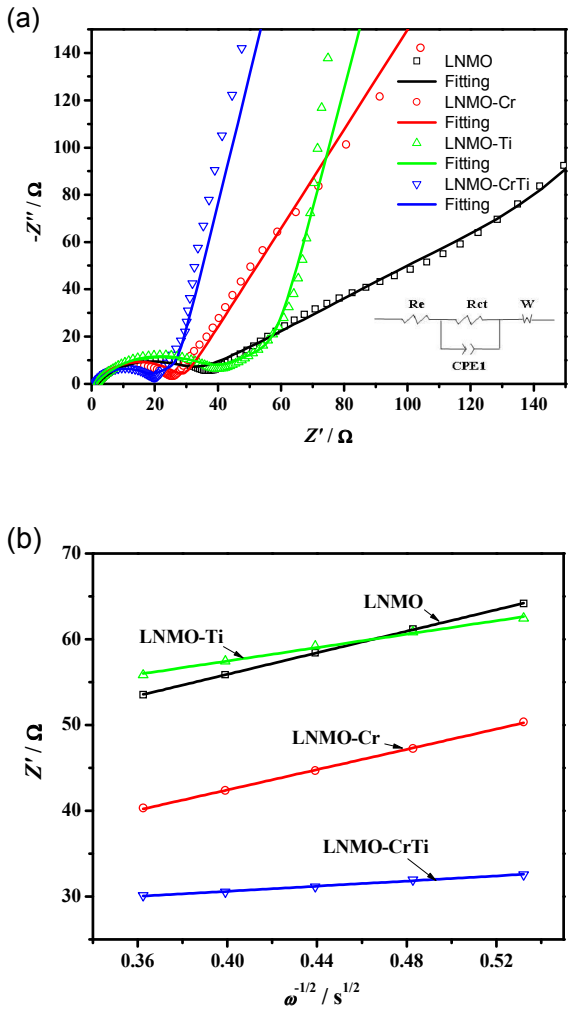

Fig. 8 Nyquist plots and fitting curves (a) and variations and fittings between Z' and the reciprocal square root of the angular frequency in the low-frequency region (b) of $LiNi_{0.45}M_{0.05}Mn_{1.5}O_4$ (M = Ni, Cr, Ti, $Cr_{0.5}Ti_{0.5}$) samples.

After linear fitting the relation plot between Z' and $\omega^{-1/2}$, as shown in Fig. 8(b), to estimate the Warburg factor σ, the apparent Li^+ ion diffusion coefficient D_{Li} can be obtained from Eq. (1). The D_{Li} values of LNMO, LNMO-Cr, LNMO-Ti and LNMO-CrTi are 8.807×10^{-11}, 1.353×10^{-10}, 2.012×10^{-10} and 5.736×10^{-10} $cm^2\ s^{-1}$, respectively, that is, the apparent Li^+ ion diffusion coefficient follows the order of $LiNi_{0.45}Cr_{0.025}Ti_{0.025}Mn_{1.5}O_4$ > $LiNi_{0.45}Ti_{0.05}Mn_{1.5}O_4$ > $LiNi_{0.45}Cr_{0.05}Mn_{1.5}O_4$ > $LiNi_{0.5}Mn_{1.5}O_4$, which is different from that of the R_{ct} values but is in good consistence with the rate capability, indicating that the Li^+ ion diffusion process in the solid phase is the rate-determining step of the discharge process of $LiNi_{0.5}Mn_{1.5}O_4$ cathode materials in this study. The larger Li^+ ion diffusion coefficient indicates that the Cr and/or Ti doping is favorable to fast Li^+ ion intercalation kinetics, resulting in their better rate capability.

Conclusions

The pristine $LiNi_{0.5}Mn_{1.5}O_4$ and doped $LiNi_{0.45}M_{0.05}Mn_{1.5}O_4$ (M = Cr, Ti, $Cr_{0.5}Ti_{0.5}$) spinels were synthesized by a solid-state method. The effects of doping Cr/Ti alone or both for Ni element on the crystalline structure, Mn^{3+} content, particle morphology and electrochemical performance of $LiNi_{0.5}Mn_{1.5}O_4$ cathode materials were systematically investigated. XRD results show that the Cr and/or Ti doping can effectively inhibit the formation of $Li_yNi_{1-y}O$ impurity phase, leading to higher phase purity of the product. FT-IR results illustrate that the Cr and/or Ti doping increases the cation disordering degree to different extent, which may be caused by the different Mn^{3+} contents resulting from the different valence of the doping ions. SEM observations find that the Cr and/or Ti doping increases the particle size distribution uniformity and decreases the average particle size. The electrochemical results show that the Cr and/or Ti doping can significantly improve the rate capability and cycling stability of the $LiNi_{0.5}Mn_{1.5}O_4$ electrode. The 1 C capacity retention rates after 100 cycles increase from 90.5% for the pristine sample to 95.6%, 97.8% and 102.1% for the Cr-, Ti- doped alone and co-doped samples, respectively. When discharged at 10 C rate, the $LiNi_{0.45}Cr_{0.025}Ti_{0.025}Mn_{1.5}O_4$, $LiNi_{0.45}Ti_{0.05}Mn_{1.5}O_4$, $LiNi_{0.45}Cr_{0.05}Mn_{1.5}O_4$ maintain 96.1%, 91.1% and 88.7% of their capacity at 0.2 C rate, higher than 86.2% of the pristine $LiNi_{0.5}Mn_{1.5}O_4$ material. EIS analysis also indicates that the Cr and/or Ti doping decreases the charge transfer resistance and increases the Li^+ ion diffusion coefficient, thus leading to the improved electrochemical performance. Among the doped samples, the Cr and Ti co-doped sample $LiNi_{0.45}Cr_{0.025}Ti_{0.025}Mn_{1.5}O_4$ exhibits the optimal overall electrochemical properties, which may be mainly ascribed to the presence of appropriate Mn^{3+} content and higher Li^+ ion diffusion coefficient.

Acknowledgements

The authors are grateful to the Natural Science Foundation of Hebei Province (Grant number E2015202356), Science & Technology Correspondent Project of Tianjin (Grant number 14JCTPJC00526), Technology Innovation Foundation Project for Outstanding Youth of Hebei University of Technology (Grant number 2013009) and Science & Technology Project of Hebei Province (Grant number 14214902D) for the financial support of this work.

References

1 J.M. Tarascon and M. Armand, *Nature*, 2001, 414, 359.

2 H. M. Wu, I. Belharouak, A. Abouimrane, Y.-K. Sun and K. Amine, *J. Power Sources*, 2010, 195, 2909.
3 E. Lee and K.A. Persson, *Energy Environ. Sci.*, 2012, 5, 6047.
4 J. Hassoun, K.-S. Lee, Y.-K. Sun and B. Scrosati, *J. Am. Chem. Soc.*, 2011, 133, 3139.
5 Y.-P. Zeng, X. Wu, P. Mei, L.-N. Cong, C. Yao, R.-S. Wang, H.-M. Xie and L.-Q. Sun, *Electrochim. Acta*, 2014, 138, 493.
6 G. Wang, J. Xie, C. Wu, S. Zhang, G. Cao and X. Zhao, *J. Power Sources*, 2014, 265, 118.
7 C. Jiao, L. Wang, Y. Zuo, P. Ni and G. Liang, *Solid State Ionics*, 2015, 277, 50.
8 Z. Yang, Y. Jiang, J.-H. Kim, Y. Wu, G.-L. Li and Y.-H. Huang, *Electrochim. Acta*, 2014, 117, 76.
9 W. Luo, *J. Alloys Compd.*, 2015, 636, 24.
10 J. Gao, J. Li, F. Song, J. Lin, X. He and C. Jiang, *Mater. Chem. Phys.*, 2015, 152, 177.
11 J.-H. Kim, S.-T. Myung, C.S. Yoon, S.G. Kang and Y.-K. Sun, *Chem. Mater.*, 2004, 16, 906.
12 Y. Liu, M. Zhang, Y. Xia, B. Qiu, Z. Liu and X. Li, *J. Power Sources*, 2014, 256, 66.
13 X. Zhu, X. Li, Y. Zhu, S. Jin, Y. Wang and Y. Qian, *J. Power Sources*, 2014, 261, 93.
14 J. Zheng, J. Xiao, X.Yu, L. Kovarik, M. Gu, F. Omenya, X. Chen, X.-Q. Yang, J. Liu, G.L. Graff, M.S. Whittingham and J.-G. Zhang, *Phys. Chem. Chem. Phys.*, 2012, 14, 13515.
15 X. Zhang, J. Liu, H. Yu, G. Yang, J. Wang, Z. Yu, H. Xie and R. Wang, *Electrochim. Acta*, 2010, 55, 2414.
16 J. Xiao, X. Chen, P.V. Sushko, M.L. Sushko, L. Kovarik, J. Feng, Z. Deng, J. Zheng, G.L. Graff, Z. Nie, D. Choi, J. Liu, J.-G. Zhang and M.S. Whittingham, *Adv. Mater.*, 2012, 24, 2109.
17 J. Song, D.W. Shin, Y. Lu, C.D. Amos, A. Manthiram and J.B. Goodenough, *Chem. Mater.*, 2012, 24, 3101.
18 K.R. Chemelewski and A. Manthiram, *J. Phys. Chem. C*, 2013, 117, 12465.
19 E.-S. Lee and A. Manthiram, *J. Mater. Chem. A*, 2013, 1, 3118.
20 J.-J. Shiu, W.K. Pang and S. Wu, *J. Power Sources*, 2013, 244, 35.
21 J.S. Chae, M.R. Jo, Y.-I. Kim, D.-W, Han, S.-M. Park, Y.-M. Kang and K.C. Roh, *J. Ind. Eng. Chem.*, 2015, 21, 731.
22 X. Yang, T. Yang, S. Liang, X. Wu and H. Zhang, *J. Mater. Chem. A*, 2014, 2, 10359.
23 M. Lin, S.H. Wang, Z.L. Gong, X.K. Huang and Y. Yang, *J. Electrochem. Soc.*, 2013, 165, A3036.
24 Y.-Z. Jin, Y.-Z. Lv, Y. Xue, J. Wu, X.-G. Zhang and Z.-B. Wang, *RSC Adv.*, 2014, 4, 57041.
25 X.Y. Feng, C. Shen, X. Fang and C.H. Chen, *J. Alloys Compd.*, 2011, 509, 3623.
26 J. Liu and A. Manthiram, *J. Phys. Chem. C*, 2009, 113, 15073.
27 R.D. Shannon, *Acta Cryst.*, 1976, A32, 751.
28 T.-F. Yi, C.-Y. Li, Y.-R. Zhu, J. Shu and R.-S. Zhu, *J. Solid State Electrochem.*, 2009, 13, 913.
29 T. Ohzuku, K. Ariyoshi, S. Takeda and Y. Sakai, *Electrochim. Acta*, 2001, 46, 2327.
30 T. Ohzuku, S. Takeda and M. Iwanaga, *J. Power Sources*, 1999, 81-82, 90.
31 M. Kunduraci and G.G. Amatucci, *J. Electrochem. Soc.*, 2006, 153, A1345.
32 M. Kunduraci, J.F. Al-Sharab and G.G. Amatucci, *Chem. Mater.*, 2006, 18, 3585.
33 L.P. Wang, H. Li, X.J. Huang and E. Baudrin, *Solid State Ionics*, 2011, 193, 32.
34 K. Ariyoshi, Y. Iwakoshi, N. Nakayama and T. Ohzuku, *J. Electrochem. Soc.*, 2004, 151, A296.
35 D.W. Shin, C.A. Bridges, A. Huq, M.P. Paranthaman and A. Manthiram, *Chem. Mater.*, 2012, 24, 3720.
36 E.-S. Lee, K.-W. Nam, E. Hu and A. Manthiram, *Chem. Mater.*, 2012, 24, 3610.
37 E.-S. Lee, A. Huq, H.-Y. Chang and A. Manthiram, *Chem. Mater.*, 2012, 24, 600.
38 M. Kunduraci and G. G. Amatucci, *J. Power Sources*, 2007, 165, 359.
39 B. Hai, A.K. Shukla, H. Duncan and G. Chen, *J. Mater. Chem. A*, 2013, 1, 759.
40 B. Kang and G. Ceder, *Nature*, 2009, 458, 190.
41 H. Ji, L. Zhang, M.T. Pettes, H. Li, S. Chen, L. Shi, R. Piner and R.S. Ruoff, *Nano Lett.*, 2012, 12, 2446.
42 X. Yu, Q. Wang, Y. Zhou, H. Li, X.-Q. Yang, K.-W. Nam, S.N. Ehrlich, S. Khalid and Y.S. Meng, *Chem. Commun.*, 2012, 48, 11537.
43 T. Ohzuku, R. Yamato, T. Kawai and K. Ariyoshi, *J. Solid State Electrochem.*, 2008, 12, 979.
44 G.B. Zhong, Y.Y. Wang, Y.Q. Yu and C.H. Chen, *J. Power Sources*, 2012, 205, 385.
45 X. Zhang, F. Cheng, J. Yang and J. Chen, *Nano Lett.*, 2013, 13, 2822.
46 Z. Chen, S. Qiu, Y. Cao, X. Ai, K. Xie, X. Hong and H. Yang, *J. Mater. Chem.*, 2012, 22, 17768.
47 H. Duncan, B. Hai, M. Leskes, C.P. Grey and G. Chen, *Chem. Mater.*, 2014, 26, 5374.
48 C. Zhu and T. Akiyama, *RSC Adv.*, 2014, 4, 10151.
49 K.R. Chemelewski, W. Li, A. Gutierrez and A. Manthiram, *J. Mater. Chem. A*, 2013, 1, 15334.
50 J.-H. Kim, N.P.W. Pieczonka, Y.-K. Sun and B.R. Powell, *J. Power Sources*, 2014, 262, 62.
51 A.D. Robertson, S.H. Lu and W.F. Howard Jr., *J. Electrochem. Soc.*, 1997, 144, 3505.
52 G.B. Zhong, Y.Y. Wang, X.J. Zhao, Q.S. Wang, Y. Yu and C.H. Chen, *J. Power Sources*, 2012, 216, 368.
53 S.-K. Hong, S.-I. Mho, I.-H. Yeo, Y. Kang and D.-W. Kim, *Electrochim. Acta*, 2015, 156, 29.
54 A. Manthiram, K. Chemelewski and E.-S. Lee, *Energy Environ. Sci.*, 2014, 7, 1339.
55 H. Liu, G. Zhu, L. Zhang, Q. Qu, M. Shen and H. Zheng, *J. Power Sources*, 2015, 274, 1180.
56 M. Kunduraci and G. G. Amatucci, *Electrochim. Acta*, 2008, 53, 4193.
57 J. Yang, X. Han, X. Zhang, F. Cheng and J. Chen, *Nano Res.*, 2013, 6, 679.
58 J. Wang, W. Lin, B. Wu and J. Zhao, *J. Mater. Chem. A*, 2014, 2, 16434.
59 J. Cabana, M. Casas-Cabanas, F.O. Omenya, N.A. Chernova, D. Zeng, M.S. Whittingham and C.P. Grey, *Chem. Mater.*, 2012, 24, 2952.
60 G.B. Zhong, Y.Y. Wang, Z.C. Zhang and C.H. Chen, *Electrochim. Acta*, 2011, 56, 6554.
61 L.Wan, Y. Deng, C. Yang, H. Xu, X. Qin and G. Chen, *RSC Adv.*, 2015, 5, 25988.
62 P. Arora, B.N. Popov and R.E. White, *J. Electrochem. Soc.*, 1998, 145, 807.
63 X.-L. Wu, Y.-G. Guo, J. Su, J.-W. Xiong, Y.-L. Zhang and L.-J. Wan, *Adv. Energy. Mater.*, 2013, 3, 1155.
64 A.L. Bard and L.R. Faulkner, *Electrochemical Methods, 2nd ed.*, Wiley, 2001.

Graphic Abstract

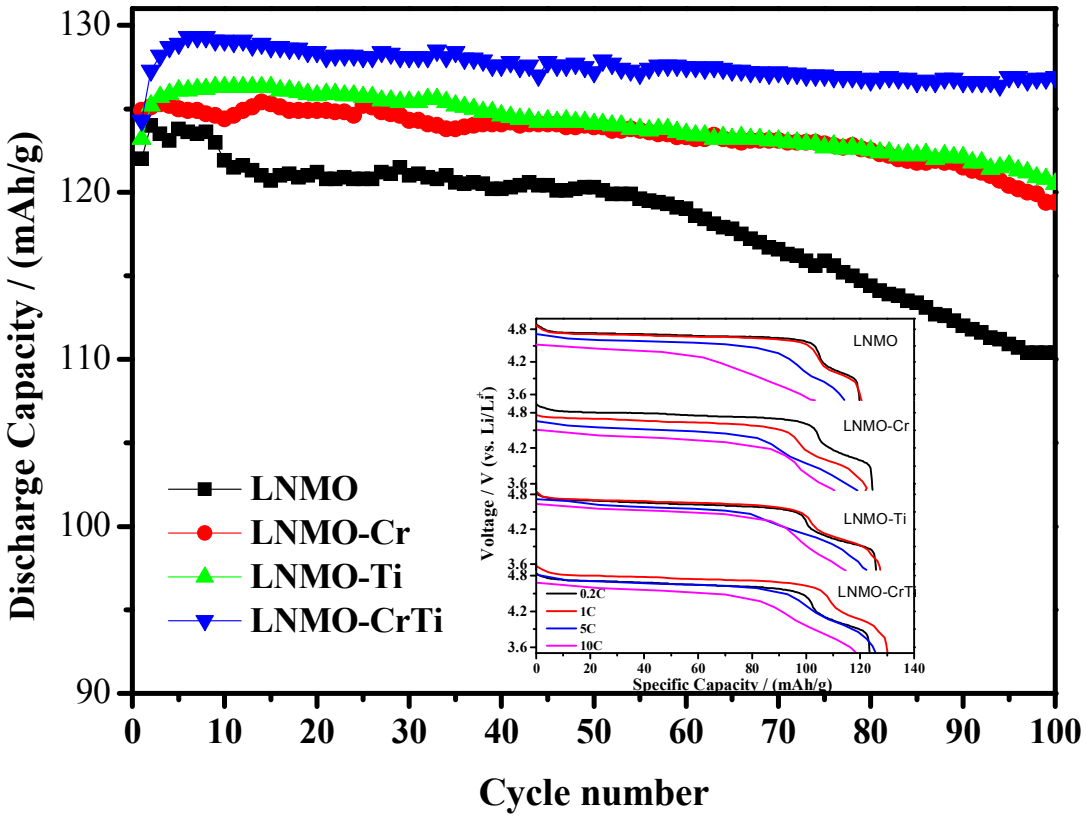

The Cr and/or Ti doping leads to the enhancement of rate capability and cycling stability. Among which, the Cr and Ti co-doped sample $LiNi_{0.45}Cr_{0.025}Ti_{0.025}Mn_{1.5}O_4$ exhibits the optimal electrochemical performance due to the presence of appropriate Mn^{3+} content and higher Li^+ ion diffusion coefficient, based on the XRD, FT-IR, SEM and EIS analysis results.